Tip/tilt estimation from defocused images

Marcos A. van Dam and Richard G. Lane

Department of Electrical and Electronic Engineering, University of Canterbury, Private Bag 4800, Christchurch, New Zealand

Received February 7, 2001; revised manuscript received July 26, 2001; accepted September 19, 2001

In astronomical imaging, the errors in the wave-front slope are a significant cause of aberrations in the detected image. We investigate how the slope can be estimated optimally using an intensity measurement of the propagated wave front. We show that the optimal location for detection of wave-front tilt is the focal plane, and we quantify the error in using defocused images, such as would be obtained from a curvature sensor, for estimating the wave-front tilt. The effect of using broadband light is also quantified. © 2002 Optical Society of America

OCIS codes: 0.10.1080, 010.1330, 010.7350.

1. INTRODUCTION

Atmospheric turbulence is known to have a dramatic effect on the resolution of ground-based optical telescopes, with the resolution often being decreased by an order of magnitude or more. Adaptive optics provides a means of recovering this lost resolution, but its performance depends on the accuracy to which the aberrations are measured. If we assume Kolmogorov turbulence, the dominant aberrations are the tip and tilt modes and together these comprise 87% of the energy of the aberrations.[1] As a consequence it is critical that these measurements be made optimally and from broadband light, since they are often made from a relatively dim source.

Our objective is to measure the angle θ that defines the least-mean-squares (LMS) slope of the wave-front. Figure 1 shows how the tip or tilt of the wave-front causes a displacement in the detected image. Teague has shown quantitatively that the tip and the tilt of the wave-front are proportional to the first-order moments of the detected intensity image.[2] In a previous paper, we investigated the optimal estimation of the slope of a wave-front at the focal plane of a telescope assuming that the turbulence is not severe.[3] This situation is of particular relevance to the Shack–Hartmann sensor, where the diameter of the aperture is typically chosen to be equal to the Fried parameter, r_0. Since r_0 is defined as the diameter of the telescope that would give a long-exposure resolution equivalent to that imposed by the atmosphere, in this case the shape of the received intensity at the focal plane is not strongly affected by the atmospheric turbulence.

In this paper we extend this analysis to the optimal estimation of the tip/tilt signal when the intensity measurements are taken at planes other than the focal plane. This is motivated, in part, by the need to analyze the performance limits of the curvature sensor for slope estimation. Curvature sensors, unlike the Shack–Hartmann sensor, take intensity measurements from defocused images. This entails a compromise since curvature-sensing measurements are more sensitive close to the focal plane, but this is at the expense of spatial resolution in the wave-front and the accuracy of the linear model.

Intuitively, we would expect tilt estimation to be affected by two main factors. The first factor is the shape of the received intensity, since we would expect to be able to estimate the center of a narrow, concentrated distribution more easily than a diffuse distribution. Second, we would like the signal being measured, the displacement of the center, to be as large as possible. These factors indicate that the accuracy of the slope estimation would be expected to degrade both with increasing distance from the focal plane and with increasing turbulence. We employ Cramér–Rao bounds to formalize this reasoning and to define the fundamental performance limits.

In Section 2 we present the optical and estimation background theory. For the general case of Fresnel diffraction, we confirm that a slope in the wave front simply causes the displacement of the image. Since the turbulence changes with time, we consider the displacement of speckle images. A speckle image is the intensity distribution of an image integrated over a period of time shorter than the atmospheric correlation time. Using prior knowledge of the intensity distribution, we derive a maximum-likelihood estimator for the displacement of the speckle image from its center. We compare this to the standard procedure for estimating the tilt by using curvature-sensing data. In Section 3 we prove that the focal plane is the optimal place to measure the slope and that as the detector moves away from the focal plane, the variance of the estimate increases. We also show that the common practice of using broadband light does not significantly affect the quality of the estimate. Simulation results are presented in Section 4 to confirm the theory that we present. Finally, we demonstrate in Section 5 that most of the energy of the boundary signal in a curvature sensor is due to higher-order aberrations, a factor that makes tip/tilt estimation difficult since it depends on the measurements of higher-order aberrations.

2. THEORY

A. Fourier and Atmospheric Optics

The first step in defining the accuracy of the tip/tilt measurement is to determine the intensity at the measure-

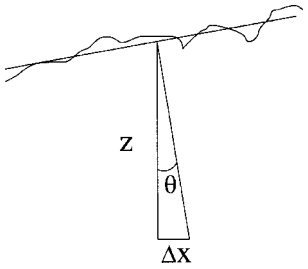

Fig. 1. Least-mean-squares slope of a wave front.

ment plane of interest. The relationship between the aberrations in the wave front at the aperture and the expected image at the detector can be modeled by using Fourier analysis.

Consider a wave of complex amplitude $U_0(\boldsymbol{\xi})$ at an aperture of diameter D. For atmospheric turbulence and the propagation distance z and wavelength λ of interest here, the complex amplitude $U_1(\mathbf{x})$ is given by the Fresnel diffraction formula:[4]

$$U_1(\mathbf{x}) = \frac{1}{i\lambda z}\exp\left(i\frac{2\pi z}{\lambda}\right)\exp\left(i\frac{\pi}{\lambda z}\mathbf{x}^2\right) \times \int_{-\infty}^{\infty} U_0(\boldsymbol{\xi})\exp\left(i\frac{\pi}{\lambda z}\boldsymbol{\xi}^2\right)\exp\left(-i\frac{2\pi}{\lambda z}\boldsymbol{\xi}\mathbf{x}\right)\mathrm{d}\boldsymbol{\xi}. \tag{1}$$

We consider the one-dimensional case first, both because it is easier to analyze and because when extended to a rectangular aperture, the two orthogonal directions can be treated individually. We follow this with results for a circular aperture.

1. Point-Spread Function

The intensity of the wave at the detector, called the point-spread function (PSF), $h(\mathbf{x})$, is $|U_1(\mathbf{x})|^2$. The PSF, when normalized to integrate to 1, defines the probability distribution of the photons as a function of position:

$$|U_1(\mathbf{x})|^2 = \left|\frac{1}{\lambda z}\int_{-\infty}^{\infty} U_0(\boldsymbol{\xi})\exp\left(i\frac{\pi}{\lambda z}\boldsymbol{\xi}^2\right)\exp\left(-i\frac{2\pi}{\lambda z}\boldsymbol{\xi}\mathbf{x}\right)\mathrm{d}\boldsymbol{\xi}\right|^2. \tag{2}$$

It is the shape of this distribution that imposes limits on our ability to estimate the wave-front slope. We can rewrite $U_0(\boldsymbol{\xi})$ as

$$U_0(\boldsymbol{\xi}) = A(\boldsymbol{\xi})\exp[i\phi(\boldsymbol{\xi})], \tag{3}$$

where $A(\boldsymbol{\xi})$ is the amplitude and $\phi(\boldsymbol{\xi})$ the phase of the wave front.

If the LMS angle of arrival of the wave front is θ, then the phase can be written as $\phi(\boldsymbol{\xi}) = \tilde{\phi}(\boldsymbol{\xi}) + (2\pi/\lambda)\theta\boldsymbol{\xi}$, where $\tilde{\phi}(\boldsymbol{\xi})$ is the zero-LMS-slope phase. Setting $\tilde{U}_0(\boldsymbol{\xi}) = A(\boldsymbol{\xi})\exp[i\tilde{\phi}(\boldsymbol{\xi})]$ leads to $U_0(\boldsymbol{\xi}) = \tilde{U}_0(\boldsymbol{\xi})\exp[i(2\pi/\lambda)\theta\boldsymbol{\xi}]$. The corresponding intensity at the detector is

$$|U_1(\mathbf{x})|^2 = \left|\frac{1}{\lambda z}\int_{-\infty}^{\infty}\tilde{U}_0(\boldsymbol{\xi})\exp\left(i\frac{\pi}{\lambda z}\boldsymbol{\xi}^2\right) \times \exp\left[-i\frac{2\pi}{\lambda z}\boldsymbol{\xi}(\mathbf{x}-\theta z)\right]\mathrm{d}\boldsymbol{\xi}\right|^2. \tag{4}$$

By comparison with Eq. (2), this shows that the effect of the wave-front slope is to displace the image by

$$\Delta\mathbf{x} = \theta z, \tag{5}$$

as shown in Fig. 1. The effect of overall slope of the wave front can be removed by recentering the speckle image, as has been noted for the geometrical optics case.[5] Centering also forms the basis of the Shack–Hartmann sensor, where the slope is estimated by the displacement of the speckle image at the focal plane.

2. Optical Transfer Function

The optical transfer function (OTF) is defined as a scaled inverse Fourier transform of the PSF,

$$\mathrm{OTF}(\boldsymbol{\xi}) = \int_{-\infty}^{\infty} h(\mathbf{x})\exp\left[i\frac{2\pi}{\lambda z}\boldsymbol{\xi}\mathbf{x}\right]\mathrm{d}\mathbf{x}, \tag{6}$$

and can be obtained by correlating the wave front at the aperture:

$$\mathrm{OTF}(\boldsymbol{\xi}) = \int_{-\infty}^{\infty} U_0(\boldsymbol{\tau}+\boldsymbol{\xi})U_0(\boldsymbol{\tau})\mathrm{d}\boldsymbol{\tau}. \tag{7}$$

The OTF can be thought of as a linear filter describing the effect of the lens and aberrations on the intensity at the measurement plane.[6] An ideal lens adds a quadratic phase shift to the incoming wave front, and is modeled by multiplying the wave front by $\exp(-i\pi\boldsymbol{\xi}^2/\lambda f)$, where f is the focal length.[4] Modifying Eq. (1) by a quadratic phase shift yields

$$h(\mathbf{x}) = \left|\frac{1}{\lambda z}\int_{-\infty}^{\infty} U_0(\boldsymbol{\xi})\exp\left[i\frac{\pi(f-z)}{\lambda f z}\boldsymbol{\xi}^2\right] \times \exp\left(-i\frac{2\pi}{\lambda z}\boldsymbol{\xi}\mathbf{x}\right)\mathrm{d}\boldsymbol{\xi}\right|^2, \tag{8}$$

and it can be seen by comparing Eq. (8) and Eq. (2) that the effective propagation distance is now $fz/(f-z)$. For a rectangular aperture we can treat the two dimensions independently. Treating $\boldsymbol{\xi}$ as one dimensional gives the defocused OTF as

$$\begin{aligned}\mathrm{OTF}_{\mathrm{lin,def}}(\xi) &= \int_{-\infty}^{\infty} P(\eta)\exp\left[i\frac{\pi(f-z)}{\lambda f z}\eta^2\right]P(\xi-\eta) \times \exp\left[-i\frac{\pi(f-z)}{\lambda f z}(\xi-\eta)^2\right]\mathrm{d}\eta \\ &= \left(1-\frac{|\xi|}{D}\right)\mathrm{sinc}\left[\frac{\pi(f-z)}{\lambda f z}\frac{|\xi|}{D}\left(1-\frac{|\xi|}{D}\right)\right] \\ &= (1-u)\mathrm{sinc}\left[\frac{\pi(f-z)}{\lambda f z}u(1-u)\right],\end{aligned} \tag{9}$$

where

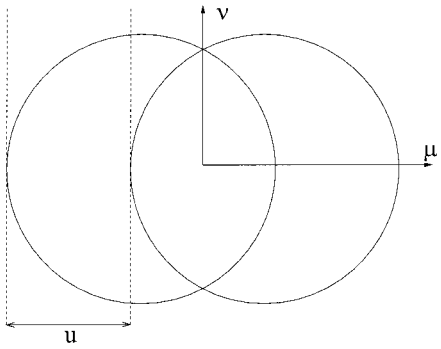

Fig. 2. Geometry to calculate the OTF of a defocused circular aperture.

$$P(\xi) = \begin{cases} 1, & \xi \in \{-D/2, D/2\} \\ 0, & \text{otherwise} \end{cases}. \tag{10}$$

Here, $\mathrm{sinc}(\xi)$ is defined as $\sin(\xi)/\xi$ and u replaces $|\xi|/D$ for clarity.

For a circular aperture, consider two circles of unit diameter displaced from each other by distance u along the μ axis, as shown in Fig. 2. The phase difference at (μ, ν) due to the quadratic phase shift of each of the two apertures is

$$\delta\phi = [(\mu + u/2)^2 + \nu^2 - (\mu - u/2)^2 - \nu^2]\frac{\pi(f - z)}{\lambda f z} = 2\mu u \frac{\pi(f - z)}{\lambda f z}. \tag{11}$$

Integrating the complex exponential over the overlapping area gives

$$\mathrm{OTF}_{\mathrm{circ,def}}(u) = \frac{4}{\pi}\int_{-(1-u)/2}^{(1-u)/2}\int_{-[1/4-(\mu+u/2)^2]^{1/2}}^{[1/4-(\mu+u/2)^2]^{1/2}} \exp\left[i 2\mu u \frac{\pi(f - z)}{\lambda f z}\right] d\nu d\mu = \frac{8}{\pi}\int_{-(1-u)/2}^{(1-u)/2}[1/4 - (\mu + u/2)^2]^{1/2}\cos\left[2\mu u \frac{\pi(f - z)}{\lambda f z}\right] d\mu. \tag{12}$$

This integral has a complicated analytical solution in terms of an infinite sum,[7] but by analogy with the linear aperture an approximation to the OTF can be derived. The triangular function in Eq. (9), $1 - u$, is replaced by the conventional OTF of a circular aperture, and the sine function by J_1, a first-order Bessel function of the first kind,[4] yielding

$$\hat{\mathrm{OTF}}_{\mathrm{circ,def}}(u) = \frac{4}{\pi}[\cos^{-1}(u) - u\sqrt{1 - u^2}]J_1\left[\frac{\pi(f - z)u(1 - u)}{\lambda f z}\right] \times \frac{\lambda f z}{\pi(f - z)u(1 - u)}. \tag{13}$$

The percentage difference between Eq. (13) and a numerical evaluation of Eq. (12) is of the order of 5% or less for all values of u. Using the Fourier transform relationship between the OTF and the PSF, Eq. (6), we can now define the intensity pattern of a defocused image.

3. Kolmogorov Turbulence

Atmospheric turbulence is usually assumed to obey Kolmogorov statistics.[8] The short-exposure OTF associated with Kolmogorov turbulence, assuming that the telescope is located in the near-field of the turbulence, is approximately given by[6]

$$\mathrm{OTF}_{\mathrm{turb}} = \exp\left[-3.44\left(\frac{uD}{r_0}\right)^{5/3}(1 - u^{1/3})\right], \tag{14}$$

where r_0 is Fried's parameter. Combining the expressions of Eq. (9) and Eq. (14) gives

$$\mathrm{OTF}_{\mathrm{turb,def}} = (1 - u)\mathrm{sinc}\left[\frac{\pi(f - z)}{\lambda f z}u(1 - u)\right] \times \exp\left[-3.44\left(\frac{uD}{r_0}\right)^{5/3}(1 - u^{1/3})\right], \tag{15}$$

and a similar expression exists for a circular aperture. Implicit in the derivation of Eq. (15) is that the quadratic phase shift due to the Fresnel propagation is orthogonal to the phase of the wave front due to the turbulence. Mathematically, we can write this condition as

$$\int_{-D/2}^{D/2}\frac{\pi(f - z)}{\lambda f z}u^2\phi(u)du = 0. \tag{16}$$

Clearly this condition is not satisfied, as the wave front can also have a defocus aberration. However it was verified that failure to satisfy Eq. (10) leads to only a small error in the OTF for the sufficiently defocused images used here. This approximation was also dealt with and numerically verified by Ellerbroek and Tyler.[9] The statistical correlation between the PSF determined by simulating an ensemble of phase screens and the PSF obtained by taking the discrete Fourier transform of Eq. (15) for a circular aperture is greater than 99%.

B. Maximum-Likelihood Estimator

A slope in the wave-front phase gives rise to a displacement of the speckle image. Consequently, slope estimation consists of deducing displacement of the image from the origin. Suppose that a photon is detected at x_0. The PSF, $h(x)$, represents the probability of a photon landing at point x; consequently, $h(x|\theta)$ is the probability of a photon landing at $x - \theta z$, given that a wave-front tilt, θ, is present. The effect of θ is simply to translate the distribution of the x_i values by θz. In order to estimate θ optimally, the form of $h(x)$ is needed. Ideally, we want to use the intensity distribution corresponding to the actual

phase screen with the LMS slope subtracted. However, this is not known *a priori*. Instead, as a best estimate to the actual intensity distribution, we use the ensemble average over many phase screens with the LMS slope subtracted. This defines the expected value of $h(x)$ and is called the short-exposure PSF (henceforth referred to as the PSF). The PSF can also be obtained by taking the Fourier transform of the OTF.

The maximum-likelihood (ML) estimator gives the estimate, $\hat{\theta}$, for the parameter, θ, that maximizes the conditional probability distribution, $h(x_0|\theta)$. For N photons, this corresponds to

$$\hat{\theta}_{\mathrm{ML}} = \max_{\theta} \left\{ \prod_{i=0}^{N-1} h(x_i|\theta) \right\}. \tag{17}$$

Equation (17) has, in general, no analytic solution and must be solved numerically.

C. Cramér–Rao Lower Bound

The Cramér–Rao lower bound (CRLB) is a lower bound on the variance of the error of an unbiased estimator. In this case, the angle of arrival, θ, is to be estimated from a measurement, x_0, given the conditional probability distribution, $h(x_0|\theta)$. The conditions that need to be satisfied are that $\partial h(x_0|\theta)/\partial\theta$ and $\partial^2 h(x_0|\theta)/\partial\theta^2$ exist and are absolutely integrable. The CRLB, which can be extended to any number of measurements, is formally stated as[10]

$$\mathrm{Var}[\hat{\theta}(x_0) - \theta] \geqslant \left(E\left\{ \left[\frac{\partial \ln h(x_0|\theta)}{\partial\theta} \right]^2 \right\} \right)^{-1}, \tag{18}$$

or equivalently

$$\mathrm{Var}[\hat{\theta}(x_0) - \theta] \geqslant \left\{ -E\left[\frac{\partial^2 \ln h(x_0|\theta)}{\partial\theta^2} \right] \right\}^{-1}. \tag{19}$$

An estimate that satisfies the equality is called an efficient estimate. The equality holds if and only if

$$\frac{\partial \ln h(x_0|\theta)}{\partial\theta} = [\hat{\theta}(x_0) - \theta]\psi(\theta), \tag{20}$$

where $\psi(\theta)$ is an arbitrary function of θ only. The bound is not, in general, the greatest lower bound, as the variance is higher if Eq. (20) is not satisfied, and tighter bounds, such as the Bhattacharyya bound, exist.[10]

The CRLB calculated above is for tilt estimation with one photon. For N measurements, the CRLB is divided by N. It can be shown that as N approaches infinity, the ML estimate becomes asymptotically efficient and approaches the CRLB.[11]

The left-hand side of Eqs. (18) and (19) can be written simply as $\mathrm{Var}[\hat{\theta}(x_0)]$, because the estimator is unbiased. The right-hand side of Eqs. (18) and (19), before inversion, can be written as

$$\int_{-\infty}^{\infty} \frac{1}{h(x_0|\theta)} \left[\frac{\partial h(x_0|\theta)}{\partial\theta} \right]^2 \mathrm{d}x_0, \tag{21}$$

and it is this expression that is used in this paper to obtain the CRLB. For the examples in this paper, the integrand of Eq. (21) has no singularities. The integral was evaluated numerically with the finite limits of integration chosen to be large enough to ensure convergence.

D. Tilt Estimation from Curvature-Sensing Measurements

Curvature sensing was introduced by Roddier[12] as a means to detect the phase of an aberrated wave front. The irradiance transport equation[13] is the basis for the wave-front reconstruction,

$$\frac{\partial I}{\partial z} = -\frac{\lambda}{2\pi}(\nabla I \cdot \nabla\phi + I\nabla^2\phi), \tag{22}$$

where $\nabla = (\partial/\partial x, \partial/\partial y)$ and $\nabla^2 = \partial^2/\partial x^2 + \partial^2/\partial y^2$. Equation (22) assumes that the geometric optics approximations are valid, which is true when λ is very small relative to the scales of interest. Two intensity images, $I_1(\mathbf{x})$ and $I_2(\mathbf{x})$, are recorded at a distance l from focus on either side of the focal plane. Assuming a small effective propagation distance, $f(f-l)/l$, it can be shown that the intensity of the images, $I_1(\mathbf{x})$ and $I_2(\mathbf{x})$, can be approximated by the following relationship[14,15]:

$$\frac{I_1(\mathbf{x}) - I_2(-\mathbf{x})}{I_1(\mathbf{x}) + I_2(-\mathbf{x})} = \frac{\lambda f(f-l)}{2\pi l}\left[\frac{\partial\phi}{\partial n}\left(\frac{f\mathbf{x}}{l}\right)\delta_c - P\nabla^2\phi\left(\frac{f\mathbf{x}}{l}\right) \right], \tag{23}$$

where P is the transmission function of the pupil, δ_c is a linear Dirac distribution around the pupil edge, and $\partial\phi/\partial n$ is the outward wave-front derivative perpendicular to the pupil edge. Equation (23) indicates that the signal is due to two terms: the contribution due to the Laplacian of the wave front and an edge signal proportional to the slope of the wave front at the edge of the aperture. The wave front is reconstructed by solving the Poisson equation with the edges of the signal providing Neumann boundary conditions. As the detector approaches the focal plane, the sensitivity of the curvature and slope measurements increases at the expense of limiting the spatial resolution in the pupil and the linearity of the model underlying Eq. (23).

A slope in the wave front causes the two speckle images to be displaced from the center by θz. Because the Laplacian of the tip and tilt terms is zero, all the information about the tip/tilt modes is contained on the boundary of the signal, and present techniques use the edge signal to estimate the slope from Eq. (23). This is achieved by integrating over the region where the two images do not overlap and subtracting the contribution to the edge signal of the higher-order terms.[16]

3. NUMERICAL RESULTS OF THE CRAMÉR–RAO LOWER BOUND

The CRLB for the estimate of the angle of arrival was found numerically from the PSF of the Fresnel-diffracted aperture. The parameters used in the calculation are $D = 1$ m, $f = 10$ m and $\lambda = 600$ nm. These calculations are performed for a single defocused image, but for the case of no scintillation in the aperture, which is approximately true at good astronomical sites,[8] the same results hold for a pair of symmetrically defocused images. In this case, both images have the same PSF but equal and

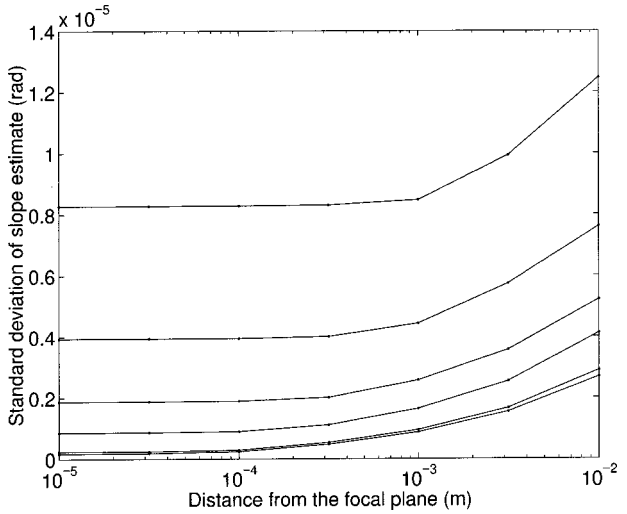

Fig. 3. CRLB of slope estimate for different levels of turbulence, $D = 1$ m and 1 photon. The curves represent, from top to bottom, $D/r_0 = 40$, 20, 10, 5, 1, and 0.

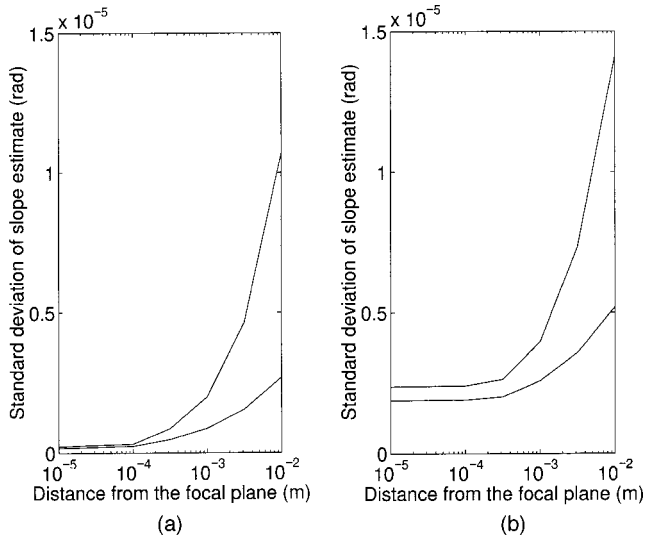

Fig. 4. CRLB of slope estimate for 300 nm $< \lambda <$ 900 nm (top curve) and $\lambda = 600$ nm (bottom curve) for (a) no turbulence and (b) $D/r_0 = 10$ at $\lambda = 600$ nm.

opposite displacements. We initially assume diffraction-limited imaging from a linear aperture of length 1 m in one dimension. This gives the bottom curve in Fig. 3, which displays the CRLB for the standard deviation of the slope estimate from one photon as a function of defocus. The minimum variance of the slope estimator starts to increase significantly for distances greater than the focal tolerance, z_R, which is given by[17]

$$z_R = 2\lambda(f/D)^2 \tag{24}$$

$$= 0.12 \text{ mm}.$$

This is expected since for measurements within z_R of the focal plane, the shape of the intensity distribution does not change significantly from that given by the Fraunhofer approximation.[17]

The CRLB calculation was repeated for wave fronts with Kolmogorov statistics. The results demonstrate that, as expected, the variance increases with increasing turbulence. Also, it is apparent that the focal plane is the best place to estimate the slope, and the more defocused the images are, the higher the minimum variance of the slope estimator. It must be emphasized that the CRLB can be approached in practice only by using detectors with a spatial resolution higher than the scale of the diffraction detail and with no read noise.

The CRLB here can be interpreted as the lower bound for an estimate from an ensemble of images with the same displacement, not just one speckle image. However, it is indicative of the amount of information about the slope contained by each photon. For a single speckle image, the instantaneous intensity differs from the PSF computed from the ensemble average. The estimate is consequently worse, because the expected intensity does not match the received intensity. In order to make the estimator optimal, we would need to know *a priori* the probability distribution of photon arrivals for that particular phase screen with the overall slope subtracted.

We now extend the analysis from the monochromatic case to broadband light. Instead of detecting at a single frequency, we allow the number of photons to be evenly distributed across a range of wavelengths, from 300 to 900 nm. This was implemented by sampling discrete wavelengths at 100 intervals, but it was verified that sampling the wavelengths more finely does not affect the results significantly. It should be noted that $r_0 \propto \lambda^{6/5}$, so as the wavelength increases, the turbulence effects decrease while the diffractive effects increase.

The CRLB is plotted in Fig. 4. From the graphs we can infer that close to the focal plane, allowing a large range of wavelengths causes only a small loss of information. As the detector moves farther away from the focal plane, the loss of information from each photon increases. However, the lost information is in the detail at very small scales of resolution, and this detail is difficult to measure in a practical sensor. We conclude that unless the source is very bright, it is better to use all the available photons to measure the tilt rather than restricting the bandwidth.

4. SIMULATIONS

In this section we discuss details of the ML- and curvature-based tilt estimation simulations and the results. Simulations were performed to confirm and quantify the behavior of the ML- and curvature-based tilt estimators from defocused images. Random phase screens consisting of circular apertures 64 pixels in diameter with Kolmogorov statistics were generated with the method of Harding *et al.*[18] Two 64 × 64 pixel speckle images were obtained with the Fresnel diffraction formula, Eq. (2), corresponding to positive and negative defocus. From these speckle images, 100 photons on average were obtained by assuming Poisson photon arrival statistics. Here, $D = 1$ m, $r_0 = 0.1$ m, $\lambda = 600$ nm and the detector array is 64 × 64. As the distance from the focal plane increases, so does the size of the speckle image. The pixel size was increased for the most defocused images so that the angular extent of the detector was larger than the angular extent of the speckle images. Hence the pixel size varied

from 6×10^{-7} rad for distances up to 1 mm from the focal plane, 12×10^{-7} rad for $l = 10^{-2.5}$ m and 24×10^{-7} rad for $l = 10^{-2}$ m. There were 1000 simulations for each level of defocus.

A. Maximum-Likelihood Estimator

The ML estimator was simulated with the PSF as the probability distribution. The PSFs were generated from the fast Fourier transforms of the OTFs. An array of 128×128 was used, which was chosen to be larger than the size of the detector to allow for the speckle image being displaced from the center as a result of the turbulence. The ML estimator was found by using a numerical maximization algorithm called the Nelder–Mead direct-search method.[19] The posterior distribution, $\Pi_{i=0}^{N-1} h(x_i|\theta)$, has no local maxima in the vicinity of the solution, so the evaluation of the estimator is independent of the algorithm used.

In wave-front sensing, the wave front, not just the slope, is estimated from the measured intensities. From the wave-front estimate, one can obtain an estimate of the speckle image with the LMS slope removed. This speckle image can then be used to define the probability distribution of photon arrival, permitting a more accurate estimate of the slope. The effects of this were quantified by repeating the ML estimation with the slope-removed speckle image defining the probability distribution. The values between the centers of adjacent pixels were found by linear interpolation.

B. Curvature Sensor

The performance of the ML estimator was compared with that of the curvature-sensor model described in Subsection 2.D. We implemented the curvature-sensor tip/tilt estimator in the manner suggested by Han, because his paper provides a detailed description of the algorithm.[16] Other authors have also suggested a similar least-squares fit of the tip/tilt terms from the edge signal.[5,20]

1. The contours of the two defocused images are obtained by truncating the speckle image where the intensity is less than 10% of the average intensity within the contour.
2. One image is inverted and subtracted from the other. The pixels where there is no overlap are obtained. These pixels are grouped into N equal bins, each representing a segment of a circle. The signed, nonoverlapping area in each segment i, A_i, is summed.
3. From Fig. 1, $\theta = \Delta\rho/z$. In polar coordinates, $A_i = \rho\Delta\rho\Delta\alpha$. We define a sensor signal, $\mathbf{s}$, where each component, s_i is given by

$$s_i = \frac{A_i}{\rho z \Delta\alpha} = \frac{2fA_i}{D(f-z)z\Delta\alpha} = \frac{NfA_i}{\pi D(f-z)z}. \tag{25}$$

4. The angle of arrival in the tip direction is now given by least-squares fitting of $\mathbf{s}$ to the average value of the cosine function over each of the segments, denoted by c:

$$\hat{\theta} = \langle \mathbf{s}, \mathbf{c}\rangle / \langle \mathbf{c}, \mathbf{c}\rangle = \frac{2Nf}{\pi D z (f-z)} \langle \mathbf{A}, \mathbf{c}\rangle. \tag{26}$$

We used 16 bins in our simulations. Note that the higher-order aberrations that contribute to the image displacement were not estimated and subtracted.

C. Results and Discussion

Figure 5 plots the results of the simulations, with 1σ error bars. One can see that it is much easier to detect the

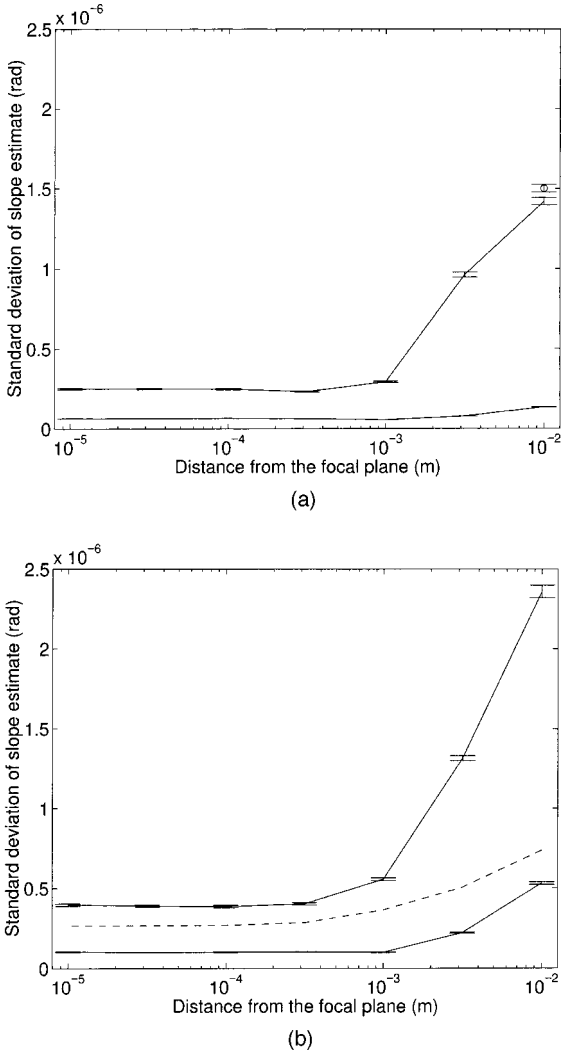

Fig. 5. Solid curves are the standard deviation of the slope estimate error with use of the ML estimator from one detector plane. The error is plotted in (a) for an infinite number of photons with the top and bottom curves corresponding to a prior distribution of the PSF and the zero LMS slope speckle image, respectively. The circle at 1.5 rad is the error using the curvature-sensing measurements. The error with 100 photons is plotted in (b) with the top and bottom curves corresponding to a prior distribution of the PSF and the zero LMS slope speckle image respectively. The dashed curve is the CRLB for 100 photons with use of the PSF.

Table 1. Effect of Zernike Polynomials on the Tip Term

Z_k	Polynomial	Derivative	$\sqrt{E[d_k^2]}$	Signal Standard Deviation
Z_2	$2\rho\cos(\alpha)$	$2\cos(\alpha)$	0.6693	1.339
Z_8	$\sqrt{8}(3\rho^3 - 2\rho)\cos(\alpha)$	$7\sqrt{8}\cos(\alpha)$	0.0787	1.559
Z_{16}	$\sqrt{12}(10\rho^5 - 12\rho^3 + 3\rho)\cos(\alpha)$	$17\sqrt{12}\cos(\alpha)$	0.0346	2.040
Z_{30}	$4(35\rho^7 - 60\rho^5 + 30\rho^3 - 4\rho)\cos(\alpha)$	$124\cos(\alpha)$	0.0208	2.581

slope close to the focal plane. The variance of the LMS slope in each of the tip/tilt directions is $7.17r_0^{-5/3}D^{-1/3}$ rad^2 m^{-2}.[1] For $r_0 = 0.1$ m and $D = 1$ m, this corresponds to an angle-of-arrival standard deviation of 1.74×10^{-6} rad in each direction, totalling 2.46×10^{-6} rad. It can be seen that if only the tip/tilt terms are estimated, the slope estimation from very defocused images is of little use.

The curvature sensor cannot be employed very close to the focal plane owing to the difficulty in defining the overlap when the images are manifestly not circular. This limits the distance from focus for the algorithm described in Subsection 4.B. and is the reason there is only one point—at a distance of 0.01 m—in Fig. 5(a) corresponding to the conventional curvature-sensing algorithm. As expected, the ML estimator performs slightly better than the curvature sensor at this distance, and in addition it can also be used closer to the focal plane.

For $N = \infty$, the mismatch between the ensemble PSF and the speckle image is the limiting factor, so the top curve in Fig. 5(a) does not go to zero. The error in estimating the LMS slope using the actual speckle image as the *a priori* probability distribution should tend to zero as the number of photons goes to infinity. However, in practice there remains an error associated with pixelation and interpolation, owing to the finite number of pixels used.

From close inspection of Fig. 5(a), there is a very small improvement in the estimate when the images are moved away from focus. We postulate that this is because a small defocus smooths the speckle images at small scales, which improves the accuracy of the subpixel interpolation.

In Fig. 5(b), we compare the one-dimensional CRLB results with the simulations. Here the CRLB from Fig. 3 needs to be divided by $\sqrt{100}$ since there are 100 photons, and multiplied by $\sqrt{2}$ because there the variance is the same in each of the two dimensions. This procedure is necessary in order to obtain an approximation to the two-dimensional CRLB. The bound is quite tight close to the focal plane compared with ML estimation with the PSF. For the two most defocused images the pixel size is increased in the simulations, so the performance relative to the CRLB degrades.

5. EFFECT OF HIGHER-ORDER ABERRATIONS ON TILT SENSING

The aberration of a wave front from a circular aperture, $\phi(\xi, \eta)$, can be described as an infinite sum of orthonormal Zernike polynomials,[1]

$$\phi(\xi, \eta) = \sum_{k=2}^{\infty} d_k Z_k(\xi, \eta), \tag{27}$$

where d_k is the coefficient of the kth Zernike polynomial, Z_k. Z_1 is constant across the aperture and is assumed to be zero. The wave-front tip and tilt terms are $Z_2 = 2\rho\cos(\alpha)$ and $Z_3 = 2\rho\sin(\alpha)$, respectively. Here $\rho = (\xi^2 + \eta^2)^{1/2}$ is the distance from the center of the aperture and α is the angle between vectors (ξ, η) and (1,0). We consider the tip term only, as the same results hold for the tilt. Assuming a circular aperture with unit radius, taking the normal derivative of the tip component gives

$$\frac{\partial Z_2}{\partial n} = 2\cos(\alpha). \tag{28}$$

However, all the other Zernike polynomials with a $\cos(\alpha)$ angular dependence also displace the speckle image. Table 1 displays the first four Zernike polynomials with a $\cos(\alpha)$ angular dependence. For each polynomial, the normal derivative at the edge is computed. This is multiplied by the standard deviation of the turbulence-induced Zernike coefficient to obtain the expected value of the standard deviation of the slope at the edge of the aperture. The values displayed are for $D/r_0 = 1$, and the standard deviation is proportional to $(D/r_0)^{5/3}$. The variances of the Zernike coefficients, $E[d_k^2]$, represent the power of each aberration and were obtained from Noll's paper.[1]

It can be seen from Table 1 that the higher-order aberrations make the most significant contributions to the slope at the edge of the aperture. The procedure for estimating the tip suggested by Han[16] is to obtain the displacement of the defocused apertures and subtract the contributions from the higher-order terms. The above analysis shows that this is difficult for Kolmogorov turbulence as it involves measuring high-order aberrations to a very high precision. The reason that the curvature-sensor tilt measurement works in practice is that the impact of the high-frequency phase components on the tilt decreases as the detector approaches the focal plane.

To illustrate the attenuation of high-frequency components, we simulated the Fresnel propagation of a 2-m linear aperture, focused 10 m away. The phase at the aperture was aberrated with each of the Zernike polynomials of Table 1. Because the simulation was in one dimension, α was set to zero. When the aberration was a tilt (Z_2), the angle of displacement of the image, θ, was equal to the angle of the wave-front slope at the edge of the aperture, $\partial(\phi\lambda/2\pi)/\partial n$. The ratio of θ to the slope angle is plotted in Fig. 6. It can be seen that as the wave propagates

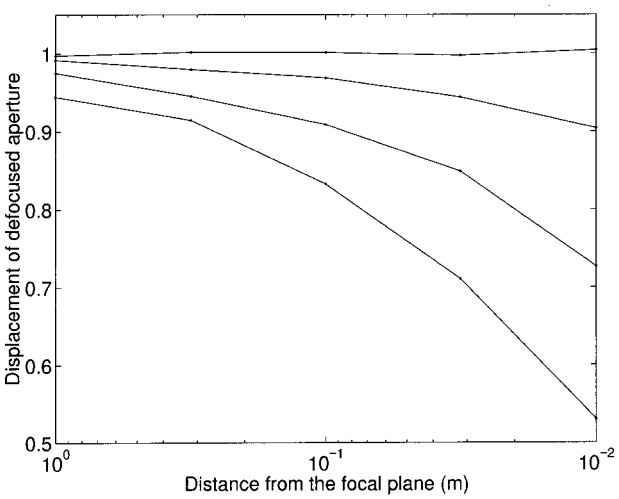

Fig. 6. Displacement of aberrated defocused aperture. The curves, from top to bottom, are for Z_2, Z_8, Z_{16}, and Z_{30}.

closer to the focal plane, the effect of the higher-order aberrations on the displacement of the image decreases. For example, if the detector is placed 1 cm away from the focal plane, the displacement due to Z_{30} is about half of what Eq. (23) predicts. The aberrations of an order higher than Z_{30} are even more attenuated, so it is possible to estimate the tilt without having to correct for a large number of higher-order aberrations. In addition, Fig. 6 suggests that the closer to the focal plane, the better the tilt estimation becomes without compensating for the other aberrations. This provides confirmation that decreasing l reduces the aliasing of the high-order aberrations onto the lower-order ones in the curvature sensor because the wave front diffracts.[14] In essence, the high-spatial-frequency components become blurred and the spatial resolution of the sensor decreases. The logical extension to this argument is to make the wave-front slope measurement at the focal plane, because then the aliasing of the high-order Zernike polynomials is reduced as much as possible.

6. CONCLUSIONS

The slope of the wave front is a critical parameter in wave-front sensing since it causes the displacement of the image intensity for the case of Fresnel diffraction. We show mathematically that the best place to estimate the tip/tilt terms is at the focal plane, and we present a ML algorithm for slope estimation from defocused images. As the detector is moved away from the focal plane, the variance of an optimal tilt estimator increases, but the spatial resolution of the curvature sensor increases. Adding a third detector at or near the focal plane could consequently be useful in estimating the wave-front slope. Furthermore estimating the LMS slope using the curvature sensing equation is very difficult for Kolmogorov turbulence, because most of the contributions to the wave-front slope at the edge come from high-frequency aberrations. This situation is alleviated by the compensation of the higher-order modes with an adaptive optics system and by the attenuation due to propagation of higher-order modes near the focal plane. Finally, unless the source is very bright, in theory as well as in practice it is best to use all the available photons rather than restrict the bandwidth.

ACKNOWLEDGEMENTS

The authors thank the Observatoire de Lyon, where this research was completed, and the New Zealand government, which provided financial aid in the form of a Bright Futures scholarship and a Marsden Fund research grant. We also thank the anonymous reviewers for useful suggestions on improving the text.

R. G. Lane may be reached at r.lane@elec.canterbury.ac.nz.

REFERENCES

1. R. J. Noll, "Zernike polynomials and atmospheric turbulence," J. Opt. Soc. Am. **66**, 207–211 (1976).
2. M. R. Teague, "Irradiance moments: their propagation and use for unique retrieval of phase," J. Opt. Soc. Am. **72**, 1199–1209 (1982).
3. M. A. van Dam and R. G. Lane, "Wave-front slope estimation," J. Opt. Soc. Am. A **17**, 1319–1324 (2000).
4. J. Goodman, *Introduction to Fourier Optics* (McGraw-Hill, San Francisco, Calif., 1968), pp. 57–100.
5. C. Roddier and F. Roddier, "Wave-front reconstruction from defocused images and the testing of ground-based optical telescopes," J. Opt. Soc. Am. A **10**, 2277–2287 (1993).
6. D. L. Fried, "Optical resolution through a randomly inhomogeneous medium for very long and very short exposures," J. Opt. Soc. Am. **56**, 1372–1379 (1966).
7. C. S. Williams and O. A. Becklund, *Introduction to the Optical Transfer Function* (Wiley, New York, 1989), pp. 291–299.
8. F. Roddier, "The effect of atmospheric turbulence in optical astronomy," in *Progress in Optics*, E. Wolf, ed. (North-Holland, Amsterdam, 1981), pp. 283–376.
9. B. L. Ellerbroek and D. W. Tyler, "Modelling the combined effect of static and varying phase distortions on the performance of adaptive optical systems," Appl. Opt. **38**, 3857–3868 (1999).
10. H. L. Van Trees, *Detection, Estimation, and Modulation Theory* (Wiley, New York, 1968), pp. 66–85, Part 1.
11. H. Cramér, *Mathematical Methods of Statistics* (Princeton U. Press, Princeton, N. J., 1946), pp. 498–505.
12. F. Roddier, "Curvature sensing and compensation: a new concept in adaptive optics," Appl. Opt. **27**, 1223–1225 (1988).
13. M. R. Teague, "Deterministic phase retrieval: a Green's function solution," J. Opt. Soc. Am. **73**, 1434–1441 (1983).
14. G. Rousset, "Wave-front sensors," in *Adaptive Optics in Astronomy*, F. Roddier, ed. (Cambridge U. Press, Cambridge, UK, 1999), pp. 91–130.
15. F. Roddier, "Wavefront sensing and the irradiance transport equation," Appl. Opt. **29**, 1402–1403 (1990).
16. I. Han, "New method for estimating wavefront from curvature signal by curve fitting," Opt. Eng. **34**, 1232–1237 (1995).
17. M. Born and E. Wolf, *Principles of Optics* (Cambridge U. Press, Cambridge, UK, 1999), p. 491.
18. C. M. Harding, R. A. Johnston and R. G. Lane, "Fast simulation of a Kolmogorov phase screen," Appl. Opt. **38**, 2161–2170 (1999).
19. J. C. Lagarias, J. A. Reeds, M. H. Wright and P. E. Wright, "Convergence properties of the Nelder-Mead simplex method in low dimensions," SIAM J. Optimiz. **9**, 112–147 (1998).
20. S. Rios, E. Acosta and S. Bara, "Modal phase estimation from wavefront curvature sensing," Opt. Commun. **123**, 453–456 (1996).